Original Article

The transcription activity of *OTX2* on *p16* expression is significantly blocked by methylation of CpG shore in non-promoter of lung cancer cell lines

Honghao Peng[1#^], Wenfan Fu[2#], Chong Chang[1], Huan Gao[1], Qianmei He[1], Ziqi Liu[1], Mengxing Cui[1], Han Wang[1], Yongjiang Yu[1], Yonghui Wu[2], Xue Zhang[1], Shuyun Jiang[1], Chi Xu[1], Xiaoyu Shen[1], Zhihan Zhang[1], Yixiang Zhou[1], Daochuan Li[1], Qing Wang[1]

[1]Guangzhou Key Laboratory of Environmental Pollution and Health Risk Assessment, Department of Toxicology, School of Public Health, Sun Yat-sen University, Guangzhou, China; [2]Department of Thoracic Surgery, Affiliated Cancer Hospital & Institute of Guangzhou Medical University, Guangzhou, China

Contributions: (I) Conception and design: H Peng, W Fu, Q Wang; (II) Administrative support: H Peng, C Chang, Q He; (III) Provision of study materials or patients: H Peng, Y Zhou, H Wang, X Shen; (IV) Collection and assembly of data: H Peng, H Gao, Z Liu; (V) Data analysis and interpretation: Y Yu, C Xu, X Zhang, S Jiang; (VI) Manuscript writing: All authors; (VII) Final approval of manuscript: All authors.

[#]These authors contributed equally to this work.

Correspondence to: Prof. Qing Wang, MD. Guangzhou Key Laboratory of Environmental Pollution and Health Risk Assessment, Department of Toxicology, School of Public Health, Sun Yat-sen University, No. 74 Zhongshan Rd 2, Guangzhou 510080, China. Email: wangq27@mail.sysu.edu.cn.

Background: The aberrant expression of the classical tumor suppressor gene *p16* is a frequent event in lung cancer mainly due to the hypermethylation of its 5'-cytosine-phosphate-guanine-3' island (Cgi). However, whether methylation happens in other regions and how *p16* expression and function are affected are largely unknown.

Methods: Clustered Regularly Interspaced Short Palindromic Repeats/dCas9 (CRISPR/dCas9) technology was used for methylation editing at specific site of *p16*. The effects of methylation editing were detected by 3-(4,5-dimethylthiazol-2-yl)-5(3-carboxymethoxyphenyl)-2-(4-sulfopheny)-2H-tetrazolium, inner salt (MTS), transwell migration and wound healing tests. Chromatin immnoprecipitation-quantitative polymerase chain reaction (CHIP-qPCR) was performed to explore the impact of Cgi shore methylation on the binding abilities of transcription factors (TFs) including *YY1*, *SP1*, *ZNF148* and *OTX2* to *p16* gene. A rescue experiment was performed to verify the regulatory effect of *OTX2* on *p16*. The negative relationship between *p16* expression and the methylation level of Cgi shore in non-promoter region was further verified with datasets from The Cancer Genome Atlas (TCGA) program and lung adenocarcinoma (LUAD) patients' samples.

Results: The suppressive effect of *p16* Cgi shore methylation on its expression was demonstrated in both HEK293 and A549 cells using CRISPR/dCas9-mediated specific site methylation editing. Methylation of the Cgi shore in the *p16* non-promoter region significantly decreased its expression and promoted cell growth and migration. The ability of *OTX2* bound to *p16* was significantly reduced by 19.35% after methylation modification. Over-expression of *OTX2* in A549 cells partly reversed the inhibitory effect of methylation on *p16* expression by 19.04%. The verification results with TCGA and LUAD patients' samples supported that the *p16* Cgi shore is a key methylation regulatory region.

Conclusions: Our findings suggested that methylation of the Cgi shore in the *p16* non-promoter region can hamper the transcriptional activity of *OTX2*, leading to a reduction in the expression of *p16*, which might contribute to the development of lung cancer.

^ ORCID: 0009-0002-8998-5637.

Keywords: *p16*; *OTX2*; DNA methylation editing; Clustered Regularly Interspaced Short Palindromic Repeats/dCas9 (CRISPR/dCas9); lung cancer

Submitted May 26, 2023. Accepted for publication Sep 13, 2023. Published online Oct 20, 2023.
doi: 10.21037/tcr-23-909
View this article at: https://dx.doi.org/10.21037/tcr-23-909

Introduction

Lung cancer is one of the most common malignant tumors globally, being a leading cause of death among cancer patients. Moreover, also it has one of the highest incidence rates, with 2.2 million new cases of lung cancer reported worldwide in 2020 (1). Although rapid progress has been made in the treatment of lung cancer, the 5-year survival rate of lung cancer remains relatively low (2). Therefore, clarifying the driving factors of lung cancer and identifying biomarkers for early prevention are effective strategies to reduce the incidence rate and mortality of lung cancer in the population.

According to previous studies, gene mutations and epigenetic variations are key drivers in tumor development (3). Abnormal epigenetic changes, such as DNA hypermethylation of specific tumor suppressor genes, serve as biomarkers of early tumor development (4). Among these genes, *p16* is a well-studied tumor suppressor gene encoded by the *CDKN2A* and is frequently hypermethylated in cancers (5). Moreover, it is reported that *p16* gene inactivation occurs in about 70% of cancer patients (6). Additionally, several studies have identified significant differences in DNA methylation levels of *p16* genes between lung cancer and normal tissues (7-9). Most of these studies utilized methylation-specific polymerase chain reaction (MSP) to assess the DNA methylation level of *p16*, but there were various 5'-cytosine-phosphate-guanine-3' (CpG) regions or sites being detected, and some of them might not be the key regulatory regions of *p16* (10). Therefore, it is essential to identify the impacts of different CpG regions in *p16* gene expression to effectively utilize *p16* methylation as a biomarker of early lung cancer.

DNA methylation often occurs in C-G dinucleotide-rich regions, which is called CpG island. 5'-cytosine-phosphate-guanine-3' island (Cgi) is mostly located in the gene promoter region (11). In the past decade, Cgi was the main region for people to study gene methylation regulation. However, recent studies have found that cancer-related DNA methylation occurs not only in Cgi, but also in the regions within 2 kb of its upstream and downstream, which is defined as Cgi shore (12). Although the CpG density of Cgi shores is lower than that of Cgi, their methylation has been shown to be important in regulating gene transcription. Rao *et al.* suggested that Cgi shore methylation could regulate the expression of caveolin-1 in breast cancer, potentially serving as a new prognostic marker for ERα-negative, basal-like breast cancer (13). Similarly, Bockmühl *et al.* demonstrated that after early-life stress, the methylation of the Cgi shore of *Nr3c1* could increase the activity of its promoter (14). Currently, most studies on *p16* methylation primarily focuses on its Cgi region, while the level and function of its Cgi shore methylation in lung cancer remain largely unknown.

Most studies have primarily observed a negative relationship between DNA methylation levels and gene expression, but obtaining direct evidence that DNA methylation affects the gene expression and function has been challenging. The difficulty lies in the lack of effective tools for editing DNA methylation in specific regions.

Highlight box

Key findings

- A remarkable discovery has been made regarding a novel methylation regulatory region associated with the classical tumor suppressor gene *p16*, opening up new avenues for the diagnosis and targeted treatment of lung adenocarcinoma (LUAD).

What is known and what is new?

- Methylation happens in other regions and how *p16* expression and function are affected are largely unknown.
- Methylation of the *p16* 5'-cytosine-phosphate-guanine-3' island (Cgi) shore in the non-promoter region inhibits gene expression by interfering with the transcriptional factor *OTX2*'s binding to *p16* DNA, promoting the malignant phenotype of A549 cells.

What is the implication, and what should change now?

- In the course of LUAD occurrence and development, the methylation of *p16* exerts its influence not only through Cgi but also through 5'-cytosine-phosphate-guanine-3' shores, potentially serving as a vital epigenetic biomarker for the progression of LUAD.

However, the recent development of a DNA methylation editing method based on Clustered Regularly Interspaced Short Palindromic Repeats/dCas9 (CRISPR/dCas9) has effectively addressed this issue (15). By expressing a fusion protein of DNA methylation modifying enzymes (such as *DNMT3A* or *TET1*) and dCas9, the CRISPR/dCas9 system allows precise localization of the DNA methylation modifying enzyme to specific gene regions, thereby altering the methylation levels without cutting the DNA strands.

In this study, we employed the CRISPR/dCas9 system to investigate the regulatory effect of Cgi shore methylation on *p16* expression and function. Subsequently, we examined the impact of transcriptional regulators binding to the Cgi shore of *p16* after region-specific methylation. Finally, we revealed the relationship between *p16* Cgi shore methylation and *p16* expression, utilizing data from The Cancer Genome Atlas (TCGA) program database and patient samples from the real clinical setting. Through this study, we aim to draw more attention to the methylation level of *p16* Cgi shore in lung cancer, as it holds promising potential as epigenetic biomarkers for the early detection and treatment of lung cancer. We present this article in accordance with the MDAR reporting checklist (available at https://tcr.amegroups.com/article/view/10.21037/tcr-23-909/rc).

Methods

Open-source data collection and processing

RNA sequencing and DNA methylation sequencing data of lung adenocarcinoma (LUAD) was downloaded from TCGA Xena (http://xena.ucsc.edu/), and processed using R Studio (4.0.2). UCSC website (http://genome.ucsc.edu/) and JASPAR database (https://jaspar.genereg.net/) were utilized to identify potential transcription factors (TFs) located on the Cgi shore of *p16*. Furthermore, a systematic literature search was conducted to validate the regulatory relationship between these TFs and the expression of *p16*. TFs that met the specified criteria were included in the subsequent investigations.

Clinical samples collection

A total of 15 pairs of human LUAD tissues and the matched paracancerous tissues were collected from the Affiliated Cancer Hospital and Institute of Guangzhou Medical University. All the included subjects were clinically and histopathologically diagnosed with LUAD. Tissues were snap-frozen in a –80 ℃ refrigerator located in School of Public Health, Sun Yat-sen University. The study was conducted in accordance with the Declaration of Helsinki (as revised in 2013). Written consents were obtained from the patients before their enrollment in this study. The human experimental study was approved by the Ethics Committee of the Affiliated Cancer Hospital & Institute of Guangzhou Medical University (No. 2020-SK05).

Cell lines and cultures

HEK293 and A549 cells were obtained from ATCC (Virginia, USA) and cultured in Dulbecco's modified Eagle medium (DMEM, GIBCO, USA). The culture media were supplemented with 10% fetal bovine serum (Biological Industries, BeitHaemek, Israel). Cells were maintained in a 5% CO_2 and 95% air incubator.

Plasmids construction and transfection

Single guide RNA (sgRNA) was designed using Feng Zhang website (https://zlab.bio/guide-design-resources) (Table S1). pSpCas9(BB)-2A-GFP (PX458) (#48138; Addgene, USA) with sgRNA was employed to assess the binding effect of sgRNA on target sites. Lentiviral plasmids, including Fuw-dCas9-Dnmt3a-P2A-tagBFP (#84569; Addgene, USA), and pgRNA-modified (#84477; Addgene, USA), were utilized to construct stable cell lines expressing sgRNA. In addition, pcDNA3.1(+) (V790-20; Invitrogen, USA) was used to construct cell lines over-expressing *OTX2*.

Bisulfite sequencing PCR (BSP)

The genomic DNA of HEK293 and A549 cells were extracted according to the operating instructions of GeneJET Genomic DNA PurificationKit (K0722; ThermoFisher, USA). BSP was conducted using the standard methods as described in the Epitect Bisulfite Kit (59104; Qiagen, Germany). PCR was carried out using primers designed through the online MethPrimer2.0 software (http://www.urogene.org/methprimer2/). T-A cloning was carried out using the pMD19-T vector (3271-C1; TaKaRa, Japan).

Quantitative real-time PCR

Total RNA was extracted using TRIzol (15596018; Invitrogen, USA) according to the manufacturer's

instructions. cDNA synthesis was performed using the ReverTra Ace® qPCR RT Kit (FSQ-101; TOYOBO, Japan). The quantitative real-time PCR (RT-qPCR) reaction system was prepared according to the instructions of SYBR®Green Realtime PCR Master Mix (QPK-201; TOYOBO, Japan).

T7E1 test

The fragment covering the sgRNA targeting sequence was amplified using Phusion high-fidelity DNA polymerase (M0530S; NEB, USA). The purified PCR product was used as a template to prepare a hybrid reaction system. After hybridization, 1 μL of T7E1 endonuclease was added to the above 19 μL hybridization reaction system, and the system was digested for 30–90 min at 37 ℃ in PCR instrument. The electrophoresis results were then subjected to gray scale analysis using Adobe PhotoshopCC2018 software.

The sorting of target cells by flow cytometer

The ultra-high-speed flow sorting system (Beckman Coulter, USA) in the Experimental Center of Zhongshan School of Medicine, Sun Yat-sen University was employed to sort the target cells containing fluorescent protein markers. The cell lines with high expression of *DNMT3A* were screened based on the fluorescence intensity of tagBFP. Similarly, the cell lines with high expression of sgRNA were screened using the fluorescence intensity of mCherry.

Chromatin immunoprecipitation (ChIP)

The ChIP assay was performed using the Pierce(tm) Magnetic ChIP Kit (26157; Invitrogen, USA), according to the manufacturer's instructions. In brief, 5×10^6 A549 cells were fixed in 1% formaldehyde for 10 min at room temperature. The fixed cells were then harvested, lysed, and sonicated using Sonics VCX130 (Sonics & Materials, USA). Immunoprecipitation was conducted using antibodies against *SP1* (07-645; Merck millipore, Germany), *ZNF148* (ab69933; Abcam, UK), *YY1* (46395; CST, USA), *OTX2* (AB9566; Merck Millipore, Germany) and rabbit IgG (Thermo Fisher, USA). PCR amplification of the precipitated DNA was performed.

MTS, transwell migration and wound healing test

For the cell proliferation assay, cells were equally seeded in 96-well plates. Cell viability was measured by MTS for 24, 48, 72 and 96 h, and the absorbance values at OD450 were measured using multi-function enzyme labeling instrument (BIOTEK, USA). Each group was analyzed in triplicate. For the analysis of cell migration, 1×10^6 cells were seeded in the upper chambers of Transwell plates (Corning, New York, USA). After incubation for 48 h, cells were fixed in 4% paraformaldehyde for 20 min and stained with 0.1% crystal violet for 30 min. Migrating cells were observed under microscope, and cells counts were performed using ImageJ. For the wound healing test, when the degree of cell fusion reached 100%, vertical scratches were made on the surface of the dish using a 1 mL tip. Pictures were taken at 0, 6, 12 and 24 h using a microscope, and changes in the scratch area were analyzed using ImageJ. Each group was set up with three replicates.

Statistical analysis

The data were presented as mean ± standard deviation (SD) and derived from a minimum of three independent experiments. Multiple experimental groups were compared using one-way analysis of variance (ANOVA), and pairwise comparisons were conducted using *t*-tests. P values less than 0.05 were defined as statistically significance.

Results

Methylation of p16 Cgi shore guided by CRISPR-dCas9 system inhibited p16 expression in HEK293 cells

The Cgi of *p16* is located in the 132–450-nt upstream of its transcriptional start site, while the region approximately 2 kb upstream and downstream of Cgi was defined as its Cgi shore. To investigate the regulatory relationship between Cgi shore methylation and *p16* mRNA expression, we designed 2 sgRNAs (sgRNA1–2) to target the upstream and downstream regions of *p16* Cgi shore (*Figure 1A*). The T7E1 assay results confirmed the successful binding of both sgRNAs to their target regions (Figure S1A). The time points for detecting the expression of *DNMT3A* and *p16* after instantaneous transfection were determined by capturing images using an inverted fluorescence microscope at different time intervals (Figure S1B-S1G). Besides, sgRNA1 and sgRNA2 significantly reduced *p16* mRNA levels after transient co-transfection with dCas-*DNMT3A* in HEK293 cells (Figure S1H). HEK293 cells stably expressed dCas9-*DNMT3A* (Figure S1I-S1K) and sgRNA1/sgRNA2 cell lines were established. The results confirmed

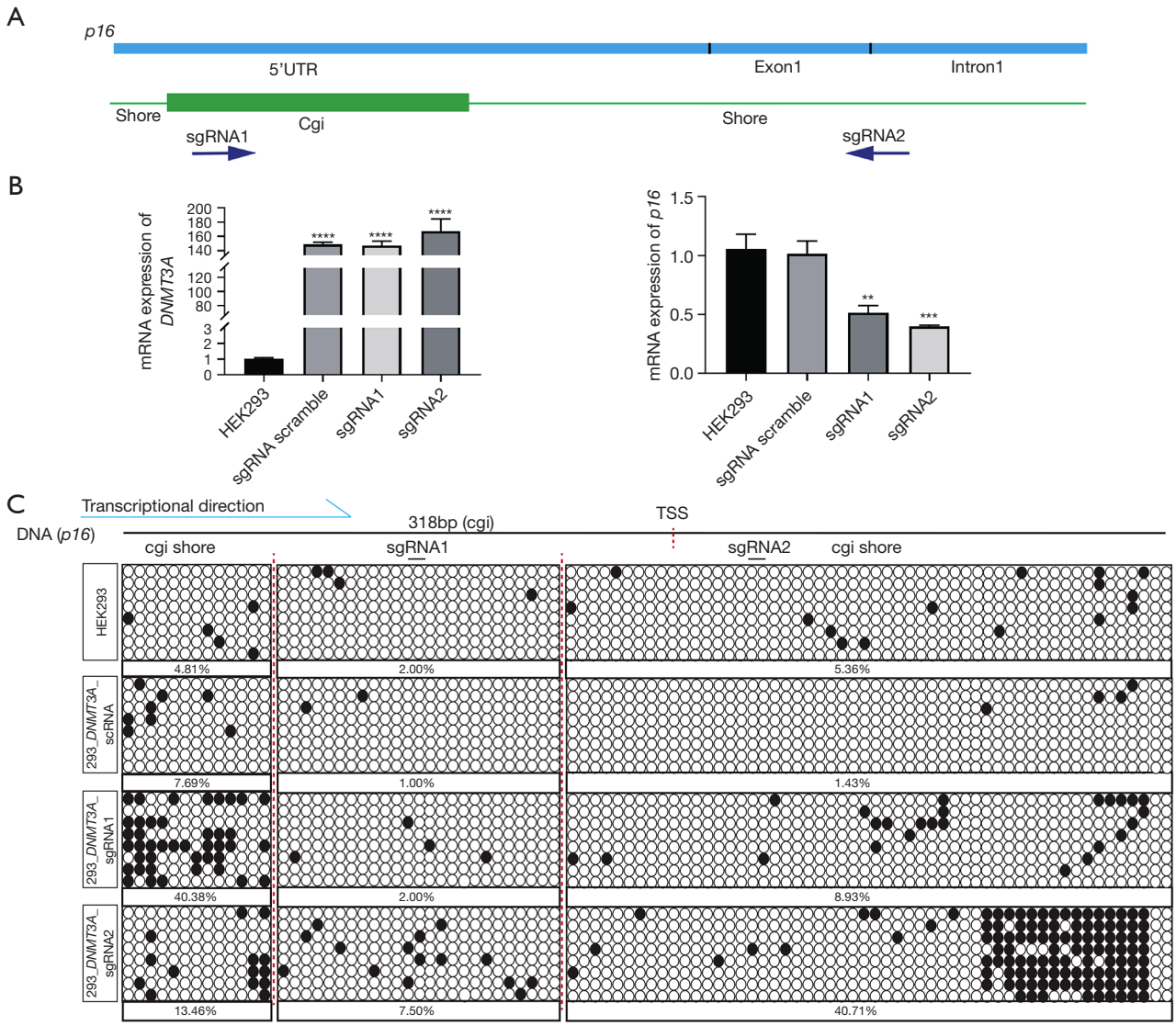

Figure 1 Increased methylation level of *p16* Cgi shore by CRISPR-dCas9 system decreased *p16* expression in HEK293 cells. (A) The blue section shows the positions of the 5'UTR, the first exon, and the first intron of *p16*. The green part shows the location of *p16* Cgi, Cgi shore and the region targeted by sgRNA. sgRNA targeting specific sequence of *p16*; sgRNA1 target to Cgi adjacent to upstream-shore (U-shore), sgRNA2 target to downstream-shore (D-shore). (B) The mRNA expression level of *DNMT3A*/*p16* in cell stably transfected of double plasmid. (C) Changes of methylation levels in targeted regions caused by targeted methylation in HEK293 cells. Each BSP sample has eight repeats, each row of circles represents the BSP sequencing results of one sample, the black solid circle indicates that the site is methylated, and the hollow circle indicates that no methylation is detected at the site. **, P<0.01; ***, P<0.001; ****, P<0.0001. Cgi, 5'-cytosine-phosphate-guanine-3' island; CRISPR-dCas9, Clustered Regularly Interspaced Short Palindromic Repeats/dCas9; 5'UTR, 5'untranslated region; sgRNA, single guide RNA; BSP, bisulfite sequencing PCR; PCR, polymerase chain reaction.

that sgRNA1 and sgRNA2 suppressed the expression levels of *p16* by 60.00% and 48.37%, respectively, compared with the control (*Figure 1B*). BSP revealed that the basal level of DNA methylation in the entire regions, including Cgi and Cgi shores of *p16*, was 3.33%. The expression of dCas9-*DNMT3A* and scramble RNA (scRNA) had little effect on it. However, in *DNMT3A*-sgRNA1 and *DNMT3A*-sgRNA2 cells, the DNA methylation levels of *p16* increased to 9.86% and 19.72% in these regions, respectively, which were significantly higher than that in the *DNMT3A*-scRNA

(*Figure 1C*). It was noteworthy that sgRNA1 predominantly altered the DNA methylation of the upstream shore of Cgi (U-shore), while sgRNA2 primarily affected the downstream shore of Cgi (D-shore) (*Figure 1C*). Compared with scRNA control, sgRNA1 and sgRNA2 increased the DNA methylation levels of U- and D-shore by 32.69% and 39.28%, respectively (*Figure 1C*). These findings indicated that the Cgi shore might be the key regulatory regions of DNA methylation in *p16*.

Hypermethylation of p16 Cgi D-shore induced by CRISPR-dCas9 system significantly promoted malignant phenotype of A549 cells

To validate the results obtained in HEK293 cells, we also constructed A549 cell lines with hypermethylated *p16* Cgi shore using the same method. Similarly, we observed significant suppression of *p16* mRNA levels by both sgRNA1 (29.62%) and sgRNA2 (82.25%) (*Figure 2A*). Similarly, we found consistent results at the protein level (*Figure 2B*). The transfection efficiency of sgRNA was verified by inverted fluorescence microscopy and flow cytometry (Figure S2A,S2B). Furthermore, we assessed DNA methylation ratio of the U-shore and D-shore in *DNMT3A*-sgRNA1 and *DNMT3A*-sgRNA2 cells. The methylation ratio of U-shore in *DNMT3A*-sgRNA1 A549 cells increased to 9.62% compared with 1.92% in scRNA cells. Similarly, the methylation ratio of the D-shore in *DNMT3A*-sgRNA2 A549 cells increased to 26.35% compared with 1.01% in scRNA cells. However, both sgRNAs did not induce changes the methylation level of *p16* Cgi (*Figure 2C*).

To explore the influence of *p16* Cgi shore hypermethylation on the phenotype of A549 cells, cell proliferation and migration tests were conducted. MTS results indicated that both *DNMT3A*-sgRNA1 and *DNMT3A*-sgRNA2 cells showed higher proliferation rates than scRNA cells 96 h after seeding (*Figure 3A*). Moreover, the wound healing test revealed a significant increase in wound closure in *DNMT3A*-sgRNA1 cells and *DNMT3A*-sgRNA2 cells compared to scRNA cells after 12 h (*Figure 3B,3C*). Additionally, the Transwell assay showed that cell migratory and invasive capabilities of *DNMT3A*-sgRNA1 and *DNMT3A*-sgRNA2 cells were significantly enhanced in comparison to scRNA cells (*Figure 3D,3E*). These findings indicated that the editing of DNA methylation levels in the Cgi shore of *p16* in A549 ells resulted in significant alterations in both the expression and biological function of *p16*.

The promotive effect of OTX2 on p16 expression was inhibited by Cgi shore methylation

Since DNA hypermethylation of the D- or U-Cgi shore can suppress the expression of *p16* and enhance the malignancy of A549 cells, the regulatory mechanism of DNA methylation on *p16* expression was investigated. Firstly, the TFs that bind to the regions of Cgi shore of *p16* were predicted by JASPAR CORE database. Subsequently, a literature retrieval was used to select the TFs that might be involved in the regulation of *p16* gene expression. Four TFs including *YY1*, *SP1*, *ZNF148* and *OTX2* were eventually screened out. According to the prediction of JASPAR CORE, there were 9 binding sites of these 4 TFs located in the Cgi shore of *p16* (*Figure 4A*). ChIP-qPCR assays were performed in *DNMT3A*-sgRNA1/sgRNA2 cells to verify whether DNA methylation changes could interfere with the binding of these TFs. The results showed that sgRNA1 could only inhibit the binding of *YY1* limitedly in U-shore, while sgRNA2 could inhibit the binding of *OTX2* in D-shore (*Figure 4B*). sgRNA1 decreased *YY1* binding level in the U-shore by 14.92%, while sgRNA2 decreased *OTX2* binding level in the D-Shore by 19.35%. In order to verify the regulatory effect of *OTX2* on *p16*, *OTX2* was over-expression in A549 *DNMT3A*-sgRNA2 cell lines. Remarkably, the high expression of *OTX2* partially restored the expression of *p16* in A549 *DNMT3A*-sgRNA2 cell line by 19.04% (*Figure 4C*). Taken together, DNA methylation on *p16* Cgi shore may regulate its gene expression by affecting the binding of *OTX2* to *p16*.

The negative correlation between p16 expression and p16 Cgi D-shore methylation was verified by the TCGA database and in LUAD tissues

To obtain the DNA methylation level of *p16* in human lung cancer, DNA methylation profiles of lung cancer tissues detected by Illumina Infinium Human Methylation 450 in TCGA database were analyzed (*Figure 5A*). The probes used to measure the DNA methylation level of *p16* cover a total of nine CpG sites. Among these nine CpG sites, cg04026675 is located in the D-shore of *p16*. Therefore, the correlation between DNA methylation and mRNA expression of *p16* was analyzed in a total of 453 LUAD tissues. Overall, the average DNA methylation of the total nine CpG sites is not negatively correlated with the mRNA

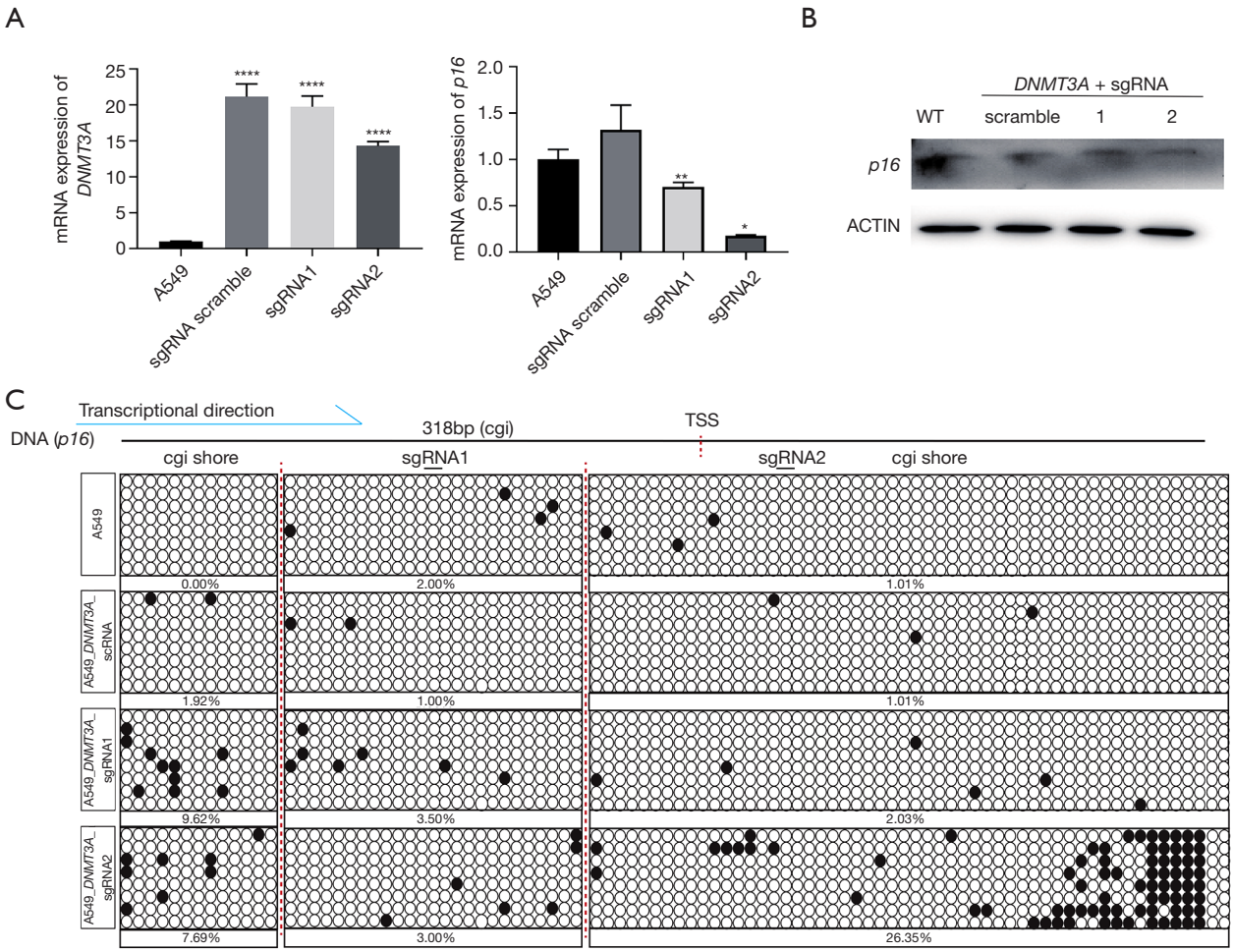

Figure 2 Increased methylation level of *p16* Cgi shore by CRISPR-dCas9 system decreased *p16* expression in A549 cells. (A) The mRNA expression level of *DNMT3A* in cell lines stably transfected of double plasmid and the effect of sgRNA transfection on mRNA expression level of *p16*. (B) *p16* protein level presented in A549 wild-type, *DNMT3A*-scRNA, DNMT3A-sgRNA1 and *DNMT3A*-sgRNA2 cells. (C) Changes of methylation levels in targeted regions caused by targeted methylation in A549 cells. Each BSP sample has eight repeats, each row of circles represents the BSP sequencing results of one sample, the black solid circle indicates that the site is methylated, and the hollow circle indicates that no methylation is detected at the site. *, P<0.05; **, P<0.01; ****, P<0.0001. Cgi, 5'-cytosine-phosphate-guanine-3' island; CRISPR-dCas9, Clustered Regularly Interspaced Short Palindromic Repeats/dCas9; sgRNA, single guide RNA; BSP, bisulfite sequencing PCR; PCR, polymerase chain reaction.

level of *p16*. However, cg04026675 in the D-shore showed remarkable negative correlation with *p16* mRNA level (r=–0.13, P=0.0044).

To further investigate the potential inverse correlation between *p16* expression and Cgi D-shore methylation, we examined the levels of *p16* expression, *p16* Cgi methylation and *p16* Cgi D-shore methylation in 15 paired LUAD and paracancerous tissues (the clinical pathological features of these samples are presented in *Table 1*). However, these clinical characteristics were not significantly associated with the level of *p16* Cgi D-shore methylation (P>0.05) (*Table 1*). A pilot study was conducted on 15 pairs of LUAD tissues. The results showed that *p16* was downregulated in 10 out of 15 pairs (66.67%, 2/3) of the LUAD tissues. In parallel, we observed that *p16* Cgi shore methylation was upregulated in 6 out of 15 pairs (40%, 2/5) compared with their adjacent control tissues. *p16* Cgi is difficult to play an important role in the regulation of *p16* due to the limited changes in the level of methylation which increased by less than 20% (*Figure 5B*). We suggested that Cgi D-shore methylation of

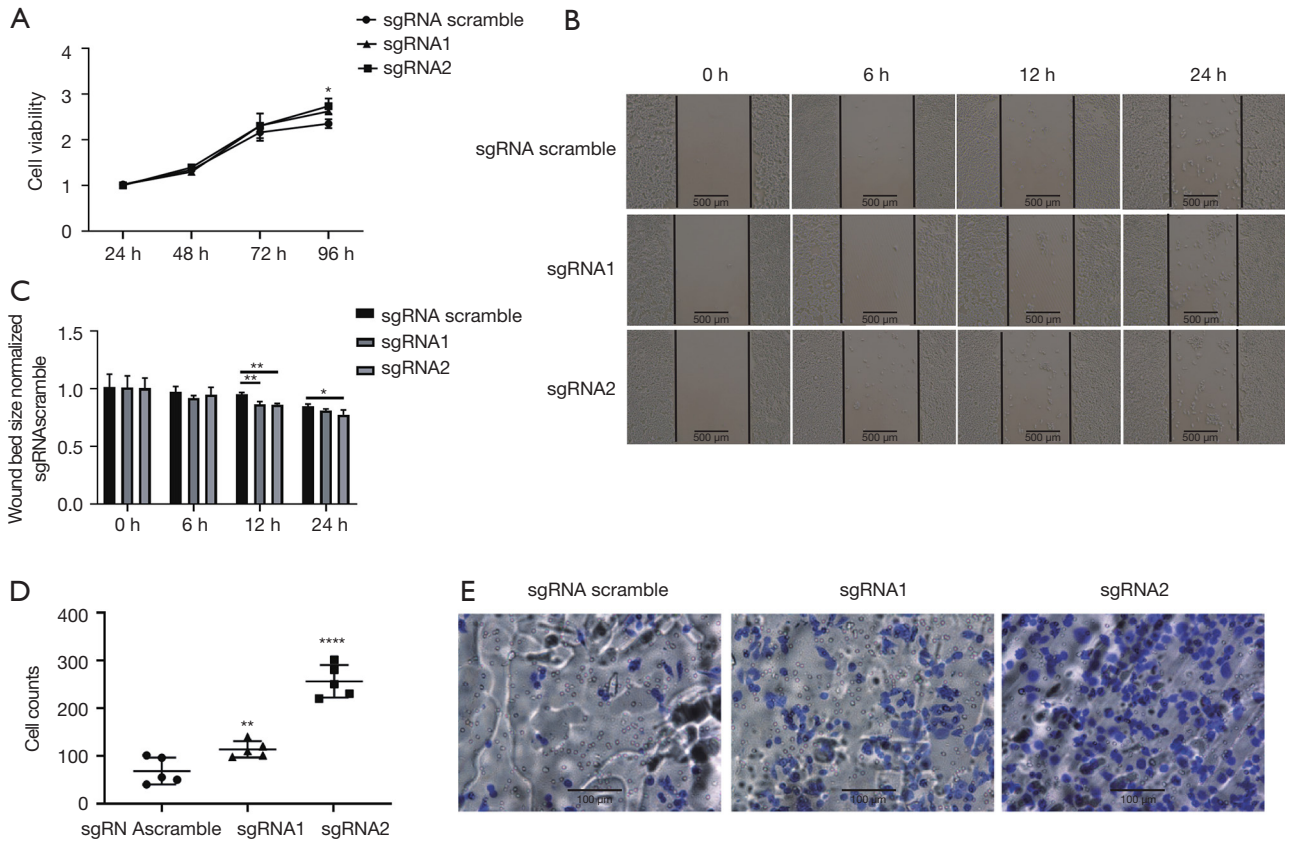

Figure 3 Increased methylation level of *p16* Cgi shore by CRISPR-dCas9 system in A549 cells affects its malignant phenotype. (A) The cell viability of three cell lines was detected by MTS at 24, 48, 72 and 96 h, respectively. (B,C) Wound healing test results for three cell lines were observed at four time points (0, 6, 12 and 24 h) after vertical scratches using a microscope and analyzed with ImageJ. (D,E) Three kinds of cell lines were seeded in Transwell 24-well plate at a density of 2×10^4 cells per well, and the results of 24 h migration experiment were stained with crystal violet and observed under a microscope. *, P<0.05; **, P<0.01; ****, P<0.0001. Cgi, 5'-cytosine-phosphate-guanine-3' island; CRISPR-dCas9, Clustered Regularly Interspaced Short Palindromic Repeats/dCas9; sgRNA, single guide RNA; BSP, bisulfite sequencing PCR; MTS, 3-(4,5-dimethylthiazol-2-yl)-5(3-carboxymethoxyphenyl)-2-(4-sulfopheny)-2H-tetrazolium, inner salt; PCR, polymerase chain reaction.

p16 may play a more important role in the regulation of *p16* function than that in Cgi through the results of population sample analysis of LUAD.

Discussion

Previous studies revealed that the Cgi of *p16* located in its promoter 132–450-nt upstream of its transcriptional start site was correlated with the expression of *p16* gene in human cancers and associated with the tumor staging and prognosis (16). Pezzuto *et al.* investigated the prognostic value of *p16* in 256 patients with non-small cell lung cancer (NSCLC) who underwent curative surgery. The research findings indicated that *p16* expression was associated with tumor grading and staging (P<0.05) and had an impact on overall survival (OS). The average OS was 36 months, but after stratifying patients based on *p16* expression levels, the OS increased to 54 months. Staging stratification showed significant prognostic value for early-stage *p16* expression (P<0.014). *P16* significantly influenced prognosis, particularly in early-stage cases, along with other variables such as tumor grading and staging (17). Although this study did not find a significant relationship between *p16* methylation levels and other variables due to the relatively small sample size (P>0.05), a significant regulatory effect of *p16* methylation on its expression level was observed.

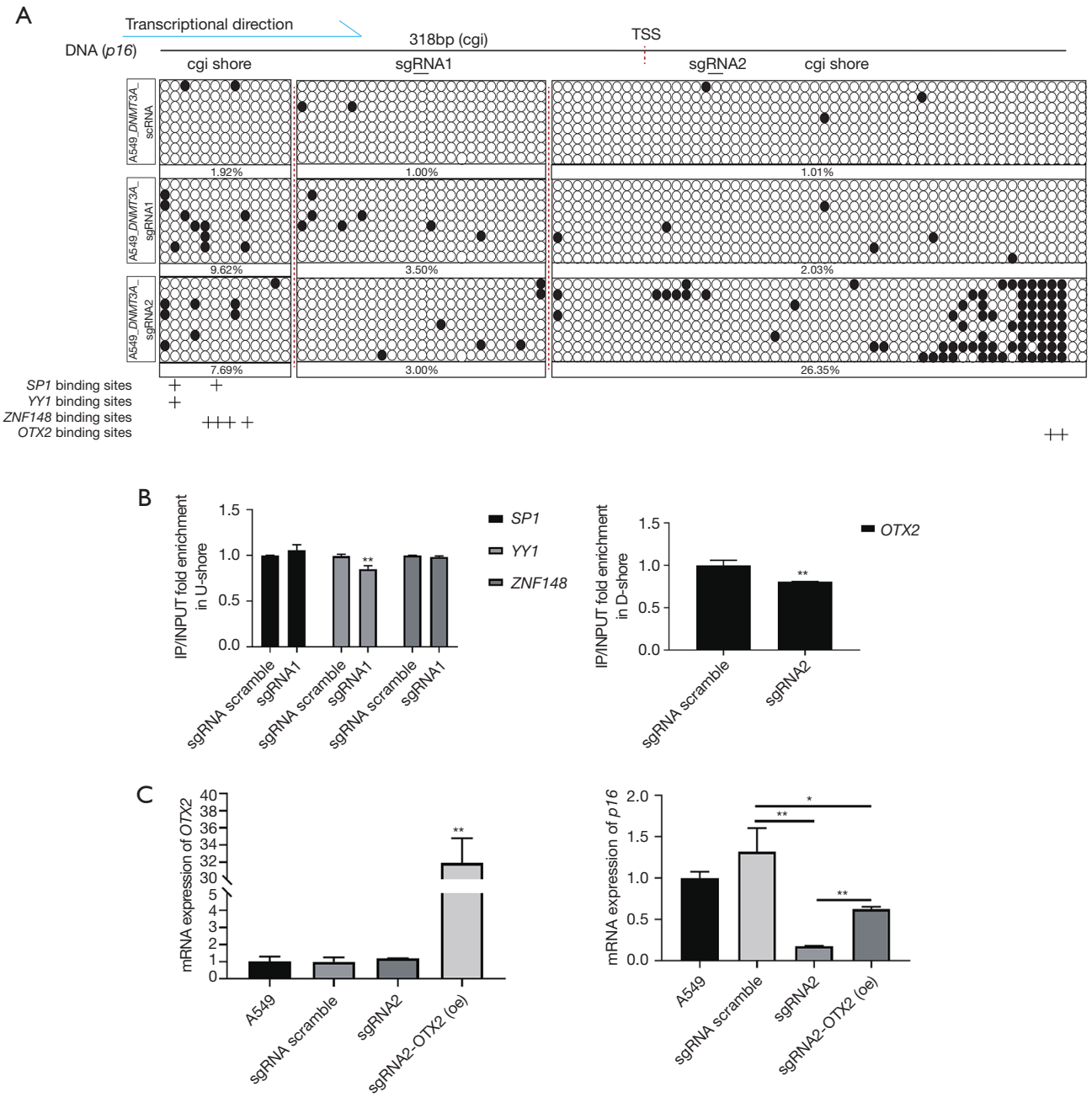

Figure 4 The elevated methylation level of *p16* Cgi shore affects the binding of key transcription factors. (A) Specific binding sites of four transcription factors on *p16* Cgi shore was described. The circle corresponding to the plus represent the CpG site contained in the transcription factor binding sequence. (B) The effects of elevated methylation levels of *p16* Cgi shore on the binding levels of four transcription factors were detected by CHIP-qPCR. The results of CHIP-qPCR were standardized by the enrichment fold of sgRNA scramble group. (C) *OTX2* was highly expressed in *DNMT3A*-sgRNA2, and the expression levels of *OTX2* and *p16* were detected. *, P<0.05; **, P<0.01. Cgi, 5'-cytosine-phosphate-guanine-3' island; CpG, 5'-cytosine-phosphate-guanine-3'; CHIP-qPCR, chromatin immunoprecipitation-quantitative polymerase chain reaction; sgRNA, single guide RNA.

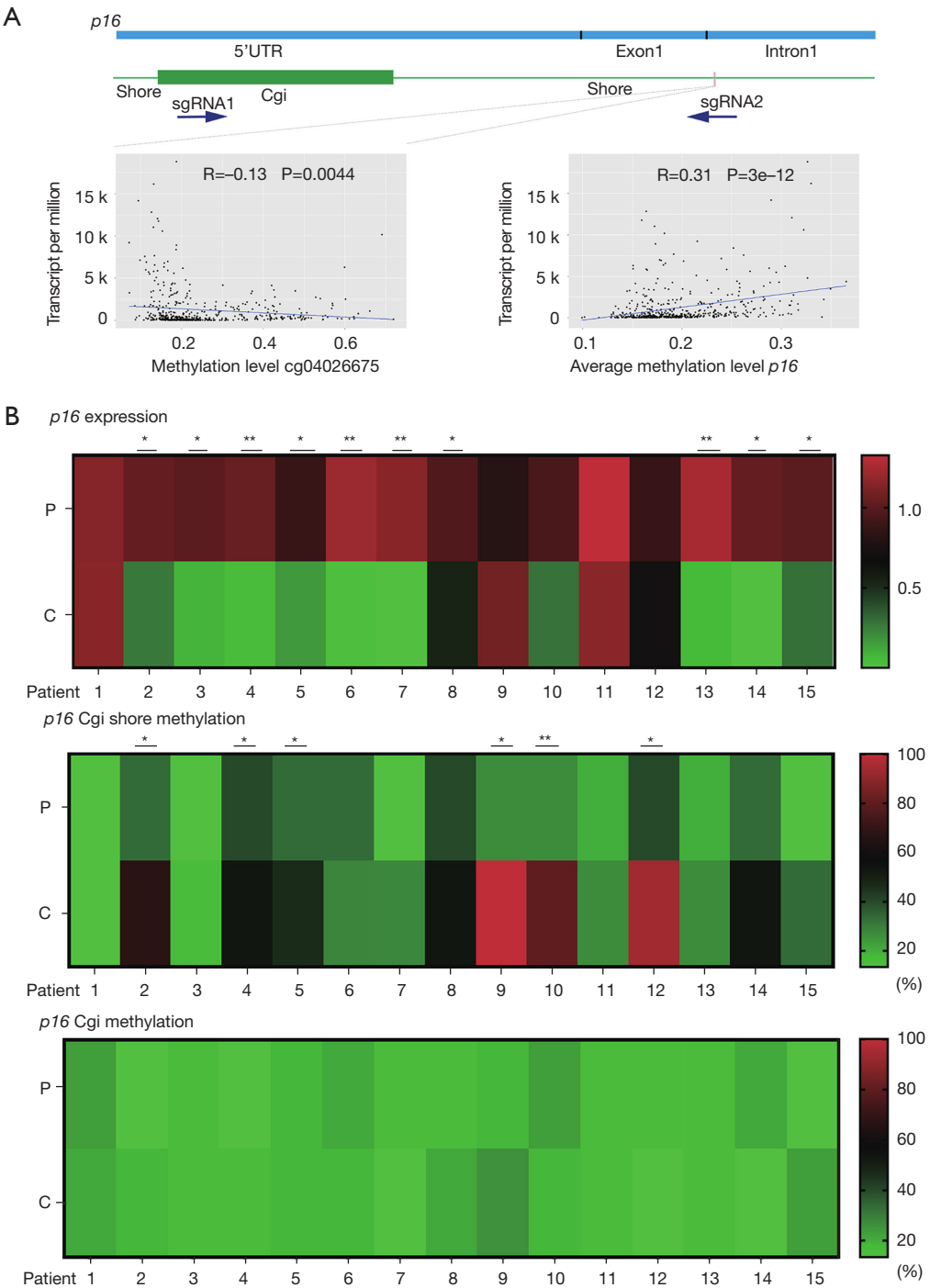

Figure 5 The importance of *p16* Cgi D-shore methylation for gene regulation was verified in TCGA program database and LUAD tissues. (A) In cancer patients, the relationship between methylation levels at *p16* Cgi D-shore and *p16* expression levels was shown in a scatter plot, in which linear fitting was performed and correlation coefficients and P values were marked. The second scatter plot shows the relationship between the average methylation level of all methylation test sites and *p16* expression in LUAD patients in the TCGA database. (B) The *p16* expression, *p16* Cgi D-shore methylation and *p16* Cgi methylation of 15 pairs samples were detected by qPCR or BSP; P stands for paracancerous tissue and C for cancer tissue. *, P<0.05; **, P<0.01. 5'UTR, 5'untranslated region; Cgi, 5'-cytosine-phosphate-guanine-3' island; TCGA, The Cancer Genome Atlas; LUAD, lung adenocarcinoma.

Table 1 The relationships between clinical characteristics and *p16* Cgi D-shore methylation

Clinical characteristics	β<0.2 (n=9)	β≥0.2 (n=6)	P value
Gender			0.6084
Male	4	4	
Female	5	2	
Age			0.6224
<60 years	6	3	
≥60 years	3	3	
Smoking			0.5804
Yes	4	1	
No	5	5	
Recurrence			0.6084
Yes	5	2	
No	4	4	
TNM stage			–
I–II	8	6	
III–IV	1	–	

Mann-Whitney *U* test was used for statistical analysis; β was defined as the degree of methylation changes; TNM, tumor node metastasis classification.

Methylation-mediated changes in *p16* expression levels may play a crucial role in affecting the prognosis of NSCLC. In their review, Pezzuto *et al.* summarized that aberrant expression of the *p16* gene was mainly observed in NSCLC, with *p16* gene methylation being the most common. High methylation of the *p16* gene, along with *p53* and *KRAS* mutations, has been reported to promote lung cancer development in smokers. Furthermore, the promoter hypermethylation of the *p16* gene leads to gene silencing, which is of great significance in confirming the downregulation of *p16* protein expression in NSCLC (18). However, more than half of NSCLC failed to be detected with *p16* Cgi methylation, indicating that the inactivation of *p16* in lung cancer might be only partially caused by abnormal DNA methylation that occurs in the *p16* Cgi region (19). Actually, methylation of Cgi shore has been shown to be inversely associated with gene expression, similar to the function of Cgi (20), However, few studies have focused on the changes of DNA methylation in regions outside the Cgi of *p16*. For example, hypermethylation of Cgi shore in *HOXA2* and *GATA2* has been inversely associated with their transcription in colon cancer (21). In our study, a new regulatory methylation region in Cgi shore of *p16* that could lead to the inhibition of its gene expression was screened. Furthermore, the analytical results with TCGA database and LUAD clinical samples demonstrated that the methylation of the *p16* Cgi D-shore was more important for the regulation of *p16* expression compared to *p16* Cgi. Although the accurate data of *p16* methylation in lung cancer need further detection, our findings provide new evidence for the study of *p16* Cgi shore methylation in lung cancer.

The regulatory mechanism of DNA methylation is considered to interfere with the binding of TFs, leading to the suppression of gene transcription (22). Numerous studies have reported a negative correlation between the global DNA methylation level and *p16* expression in lung cancer; however, the detailed mechanism was not fully clarified (23,24). Previous studies have indicated *YY1*, *SP1*, *CTCF*, *ZNF148* as important transcriptional factors of *p16* (6). In this study, four TFs of which the binding sites were located in the Cgi shore of *p16* according to the prediction results from the JASPAR database, were screened for further exploration. Previous studies have indicated that *SP1*, *YY1*, *ZNF148*, and *OTX2* can directly or indirectly regulate the expression of *p16*, however, the underlying mechanisms by which these TFs regulate *p16* expression remain unclear (25-29). Previous studies have shown that *SP1* and *OTX2* are known transcriptional activators, while *YY1* and *ZNF148* function as transcriptional suppressors. The more significant decrease in *p16* expression observed in *DNMT3A*-sgRNA2 cell line may be attributed to the decrease in *OTX2* binding levels as a transcriptional activator in the D-shore. However, it is essential to acknowledge that the level of gene expression is not solely determined by TF binding, as multiple regulatory mechanisms can influence gene expression, such as epigenetic modifications, chromatin accessibility, and post-transcriptional regulation (30). This could be a potential explanation for why the decrease in *YY1* binding did not result in an increase in *p16* mRNA expression level. Additionally, several studies have consistently shown that *ZNF148* plays a crucial role as a TF in regulating *p16* expression (26,31,32). However, the impact of methylation on *ZNF148*'s function remains uncertain. The binding sites of *ZNF148* on the *p16* gene are predominantly concentrated in the promoter region and its upstream regions. Methylation alterations downstream of the *p16* promoter may not significantly influence *ZNF148*'s ability to regulate *p16* expression. Based on our results,

we believed that the methylation of Cgi shore probably disrupted the binding of TFs described above, which might be the main reason resulting in the repression of *p16* expression.

It is known that aberrant DNA methylation is one of the early events that occurs during human cancer development (33). The hypomethylation of the genomic DNA and the hypermethylation of specific genes are the characteristics of tumors relative to normal tissues. Thus, it is widely accepted that abnormal DNA methylation changes is probably the driving factors for tumorigenesis. *P16*, being a well-studied tumor suppressor gene, is frequently inactivated in cancers through aberrant hypermethylation. However, it remains unclear whether this hypermethylation is the "driver" or "passenger" for cancer development, mainly due to lack of technology for editing DNA methylation in specific regions. In a previous study, engineered zinc finger methyltransferase was uses to increase the promoter methylation of *p16*, resulting in a significant decrease in *p16* expression by 50.6% and 57.1% in HEK293 and BGC823 cells, respectively (21). However, the previous editing approach using engineered zinc finger methyltransferase was non-specific, leading in an increase in the methylation level of approximately 900bp regions in both the *p16* promoter and exon-1. To address this limitation, the CRISPR/Cas9 system provides a promising approach for studying the methylation regulatory machinery of specific regions in the target DNA, allowing for more precise and efficient regulation of DNA methylation. According to data from TCGA, the methylation levels of *p16* were found to be 9.2% and 10.7% in normal and primary tumor tissues, respectively, in LUAD. Therefore, the significant role of *p16* in the development and progression of LUAD cannot be solely attributed to these minor changes in methylation levels. Therefore, it is difficult to differentiate between LUAD and normal tissues solely based on *p16* Cgi methylation, which is a commonly used method for detecting cancer in humans (19). To gain a deeper understanding, it is essential to investigate which specific region of *p16* is crucial for DNA methylation to exert its function, as along with exploring the underlying mechanism involved.

There is still room for improvement in this study. For instance, cell experiments cannot fully replicate the cellular environment within the human body, which may result in variations in the expression level of *p16* between the A549 cell line and lung adenocarcinoma tissue. LUAD is known for its significant genetic heterogeneity, and different patients may harbor distinct genetic alterations (34). This variability in genetic profiles among LUAD tissues might result in diverse *p16* expression patterns. The tumor microenvironment in LUAD tissues can influence gene expression levels (35). Interactions between tumor cells and surrounding stromal and immune cells can affect the expression of various genes, including *p16*. Regulatory mechanisms, such as mRNA stability, alternative splicing, and microRNA-mediated regulation, can impact gene expression levels. These mechanisms may differ between LUAD tissues and cell lines, leading to varied *p16* expression. Epigenetic changes, including DNA methylation and histone modifications, can affect gene expression (36). Differences in epigenetic patterns between LUAD tissues and cell lines may contribute to the observed variation in *p16* expression. While cell experiments may not fully replicate the human environment, they can offer valuable insights to guide subsequent animal and clinical studies. Furthermore, the impact of *p16* promoter methylation on its expression should be investigated with larger sample sizes and across various disease types to offer more comprehensive guidance for early clinical diagnosis and targeted therapy.

Conclusions

In conclusion, our study highlights the significance of DNA methylation in the Cgi D-shore of *p16* as a crucial regulator of its gene expression and function in lung cancer. The hypermethylation of *p16* Cgi D-shore suppresses its expression, thereby promoting the development of lung cancer by disrupting the binding of TF *OTX2*. Our findings have deepened the understanding of the regulation mechanisms of *p16* DNA methylation and discovered its potential as a promising target for the diagnosis and treatment of lung cancer.

Acknowledgments

Funding: This work was supported by National Natural Science Foundation of China (No. 81872656); National Natural Science Foundation of China (No. 82073583); National Key Research and Development Program of China (No. SQ2019YFC1604603).

Footnote

Reporting Checklist: The authors have completed the MDAR

reporting checklist. Available at https://tcr.amegroups.com/article/view/10.21037/tcr-23-909/rc

Data Sharing Statement: Available at https://tcr.amegroups.com/article/view/10.21037/tcr-23-909/dss

Peer Review File: Available at https://tcr.amegroups.com/article/view/10.21037/tcr-23-909/prf

Conflicts of Interest: All authors have completed the ICMJE uniform disclosure form (available at https://tcr.amegroups.com/article/view/10.21037/tcr-23-909/coif). The authors have no conflicts of interest to declare.

Ethical Statement: The authors are accountable for all aspects of the work in ensuring that questions related to the accuracy or integrity of any part of the work are appropriately investigated and resolved. The study was conducted in accordance with the Declaration of Helsinki (as revised in 2013). Written consents were obtained from patients before participation in this study. The human experimental study has received approval from the Ethics Committee of the Affiliated Cancer Hospital & Institute of Guangzhou Medical University (No. 2020-SK05).

References

1. Bade BC, Dela Cruz CS. Lung Cancer 2020: Epidemiology, Etiology, and Prevention. Clin Chest Med 2020;41:1-24.
2. Schenk EL, Patil T, Pacheco J, et al. 2020 Innovation-Based Optimism for Lung Cancer Outcomes. Oncologist 2021;26:e454-72.
3. Nam AS, Chaligne R, Landau DA. Integrating genetic and non-genetic determinants of cancer evolution by single-cell multi-omics. Nat Rev Genet 2021;22:3-18.
4. Costa-Pinheiro P, Montezuma D, Henrique R, et al. Diagnostic and prognostic epigenetic biomarkers in cancer. Epigenomics 2015;7:1003-15.
5. Esteller M. Aberrant DNA methylation as a cancer-inducing mechanism. Annu Rev Pharmacol Toxicol 2005;45:629-56.
6. Rayess H, Wang MB, Srivatsan ES. Cellular senescence and tumor suppressor gene p16. Int J Cancer 2012;130:1715-25.
7. Kurakawa E, Shimamoto T, Utsumi K, et al. Hypermethylation of p16(INK4a) and p15(INK4b) genes in non-small cell lung cancer. Int J Oncol 2001;19:277-81.
8. Sterlacci W, Tzankov A, Veits L, et al. A comprehensive analysis of p16 expression, gene status, and promoter hypermethylation in surgically resected non-small cell lung carcinomas. J Thorac Oncol 2011;6:1649-57.
9. Yanagawa N, Tamura G, Oizumi H, et al. Promoter hypermethylation of tumor suppressor and tumor-related genes in non-small cell lung cancers. Cancer Sci 2003;94:589-92.
10. Bearzatto A, Conte D, Frattini M, et al. p16(INK4A) Hypermethylation detected by fluorescent methylation-specific PCR in plasmas from non-small cell lung cancer. Clin Cancer Res 2002;8:3782-7.
11. Ren XY, Wen X, Li YQ, et al. TIPE3 hypermethylation correlates with worse prognosis and promotes tumor progression in nasopharyngeal carcinoma. J Exp Clin Cancer Res 2018;37:227.
12. Sun X, Han Y, Zhou L, et al. A comprehensive evaluation of alignment software for reduced representation bisulfite sequencing data. Bioinformatics 2018;34:2715-23.
13. Rao X, Evans J, Chae H, et al. CpG island shore methylation regulates caveolin-1 expression in breast cancer. Oncogene 2013;32:4519-28.
14. Bockmühl Y, Patchev AV, Madejska A, et al. Methylation at the CpG island shore region upregulates Nr3c1 promoter activity after early-life stress. Epigenetics 2015;10:247-57.
15. Liu XS, Wu H, Ji X, et al. Editing DNA Methylation in the Mammalian Genome. Cell 2016;167:233-247.e17.
16. Kanyama Y, Hibi K, Nakayama H, et al. Detection of p16 promoter hypermethylation in serum of gastric cancer patients. Cancer Sci 2003;94:418-20.
17. Pezzuto A, Cappuzzo F, D'Arcangelo M, et al. Prognostic Value of p16 Protein in Patients With Surgically Treated Non-small Cell Lung Cancer; Relationship With Ki-67 and PD-L1. Anticancer Res 2020;40:983-90.
18. Pezzuto A, D'Ascanio M, Ricci A, et al. Expression and role of p16 and GLUT1 in malignant diseases and lung cancer: A review. Thorac Cancer 2020;11:3060-70.
19. Jurisic V, Obradovic J, Nikolic N, et al. Analyses of

P16(INK4a) gene promoter methylation relative to molecular, demographic and clinical parameters characteristics in non-small cell lung cancer patients: A pilot study. Mol Biol Rep 2023;50:971-9.
20. Ji H, Ehrlich LI, Seita J, et al. Comprehensive methylome map of lineage commitment from haematopoietic progenitors. Nature 2010;467:338-42.
21. Cui C, Gan Y, Gu L, et al. P16-specific DNA methylation by engineered zinc finger methyltransferase inactivates gene transcription and promotes cancer metastasis. Genome Biol 2015;16:252.
22. Yin Y, Morgunova E, Jolma A, et al. Impact of cytosine methylation on DNA binding specificities of human transcription factors. Science 2017;356:eaaj2239.
23. Brock MV, Hooker CM, Ota-Machida E, et al. DNA methylation markers and early recurrence in stage I lung cancer. N Engl J Med 2008;358:1118-28.
24. Kondo K, Takahashi Y, Hirose Y, et al. The reduced expression and aberrant methylation of p16(INK4a) in chromate workers with lung cancer. Lung Cancer 2006;53:295-302.
25. Chan HM, La Thangue NB. p300/CBP proteins: HATs for transcriptional bridges and scaffolds. J Cell Sci 2001;114:2363-73.
26. Feng Y, Wang X, Xu L, et al. The transcription factor ZBP-89 suppresses p16 expression through a histone modification mechanism to affect cell senescence. FEBS J 2009;276:4197-206.
27. Sivagurunathan S, Arunachalam JP, Chidambaram S. PIWI-like protein, HIWI2 is aberrantly expressed in retinoblastoma cells and affects cell-cycle potentially through OTX2. Cell Mol Biol Lett 2017;22:17.
28. Wang X, Feng Y, Xu L, et al. YY1 restrained cell senescence through repressing the transcription of p16. Biochim Biophys Acta 2008;1783:1876-83.
29. Wang X, Pan L, Feng Y, et al. P300 plays a role in p16(INK4a) expression and cell cycle arrest. Oncogene 2008;27:1894-904.
30. Zhang Q, Huang Z, Zuo H, et al. Chromatin Accessibility Predetermines Odontoblast Terminal Differentiation. Front Cell Dev Biol 2021;9:769193.
31. Zhang CZ, Chen GG, Lai PB. Transcription factor ZBP-89 in cancer growth and apoptosis. Biochim Biophys Acta 2010;1806:36-41.
32. Zou ZV, Gul N, Lindberg M, et al. Genomic profiling of the transcription factor Zfp148 and its impact on the p53 pathway. Sci Rep 2020;10:14156.
33. Pan Y, Liu G, Zhou F, et al. DNA methylation profiles in cancer diagnosis and therapeutics. Clin Exp Med 2018;18:1-14.
34. Yang C, Zhang J, Xie J, et al. Identification of Cancer Stem Cell-related Gene by Single-cell and Machine Learning Predicts Immune Status, Chemotherapy Drug, and Prognosis in Lung Adenocarcinoma. Curr Stem Cell Res Ther 2023. [Epub ahead of print]. doi: 10.2174/1574888X18666230714151746.
35. Shao MM, Zhai K, Huang ZY, et al. Characterization of the alternative splicing landscape in lung adenocarcinoma reveals novel prognosis signature associated with B cells. PLoS One 2023;18:e0279018.
36. Liu T, Yu S, Hu T, et al. Comprehensive analyses of genome-wide methylation and RNA epigenetics identify prognostic biomarkers, regulating the tumor immune microenvironment in lung adenocarcinoma. Pathol Res Pract 2023;248:154621.

Cite this article as: Peng H, Fu W, Chang C, Gao H, He Q, Liu Z, Cui M, Wang H, Yu Y, Wu Y, Zhang X, Jiang S, Xu C, Shen X, Zhang Z, Zhou Y, Li D, Wang Q. The transcription activity of *OTX2* on *p16* expression is significantly blocked by methylation of CpG shore in non-promoter of lung cancer cell lines. Transl Cancer Res 2023;12(10):2582-2595. doi: 10.21037/tcr-23-909

Supplementary

Table S1 sgRNAs sequence and its targeting region

sgRNA targeting the *p16* promoter	5' to 3'	Position (Human hg38)
PX458-sgRNA1	Forward: TTGGTCCTCCTTCCTTGCCAACGC	chr9:21975143-21975162
	Reverse: AAACGCGTTGGCAAGGAAGGAGGA	
PX458-sgRNA2	Forward: TTGGGTGGCCAGCCAGTCAGCCGA	chr9:21974775-21974797
	Reverse: AAACTCGGCTGACTGGCTGGCCAC	
pgRNA-sgRNA1	Forward: CACCGTCCTCCTTCCTTGCCAACGC	chr9:21975143-21975162
	Reverse: AAACGCGTTGGCAAGGAAGGAGGAC	
pgRNA-sgRNA2	Forward: CACCGGTGGCCAGCCAGTCAGCCGA	chr9:21974775-21974797
	Reverse: AAACTCGGCTGACTGGCTGGCCACC	
pgRNA-sgRNA scramble	Forward: TTGGCCCCCGGGGGAAAAATTTTT	None
	Reverse: AAACAAAAATTTTTCCCCCGGGGG	

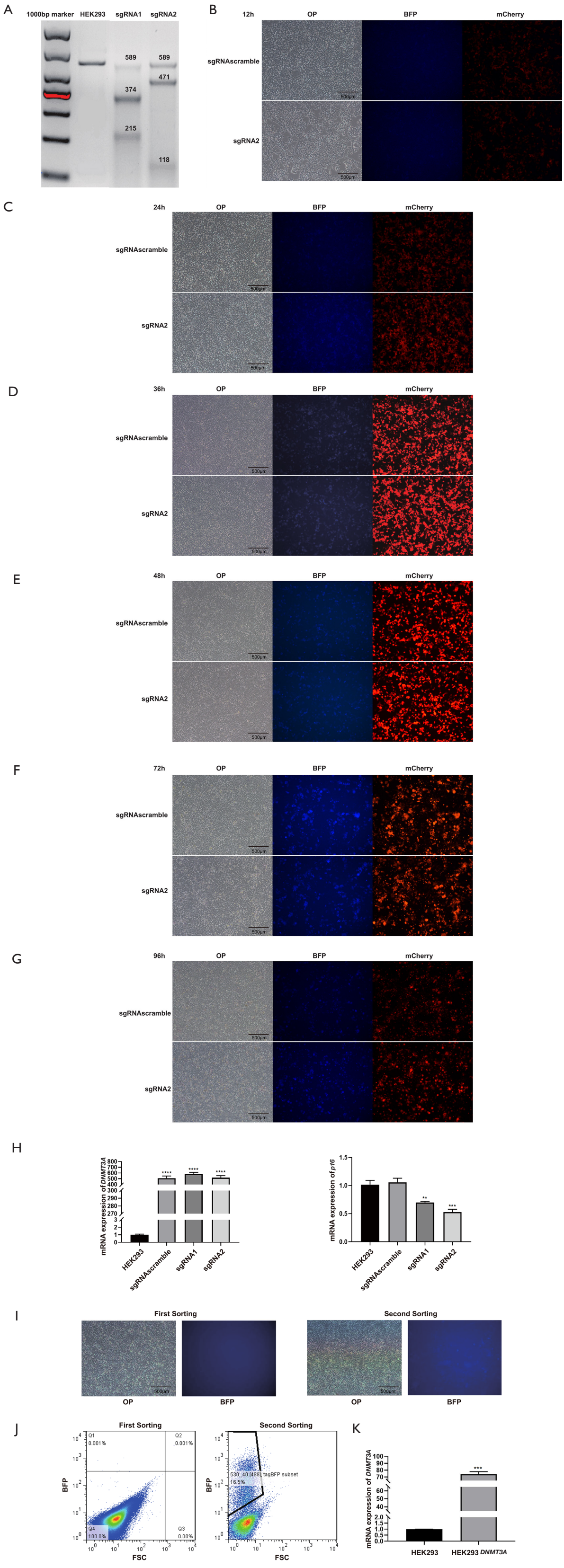

Figure S1 HEK293 cell line with stable expression of *DNMT3A* and sgRNA was constructed. (A) The cutting efficiency of Cas9 guided by sgRNA1/sgRNA2 were verified by T7E1 test. (B-G) dCas9-Dnmt3a-tagBFP and pgRNAmodified-sgRNAscramble/pgRNA-modified-sgRNA2 were transfected transiently in HEK293; pictures were taken under inverted fluorescence microscope at 12, 24, 48, 72 and 96 h, respectively (BFP and mCherry). (H) Changes of *p16* and *DNMT3A* mRNA in HEK293 cells after 48 h of transient transfection. (I,J) dCas9-*DNMT3A*-tagBFP was transfected into HEK293 cells stably. Then flow cytometry sorting was performed twice to increase positive rate of BFP. The fluorescence intensity of BFP was recorded using an inverted fluorescence microscope after sorted twice by flow cytometry, respectively. (K) The expression level of *DNMT3A* in sorted cells was verified by qPCR. **, P<0.01; ***, P<0.001; ****, P<0.0001. sgRNA, single guide RNA; OP, optical picture; FSC, forward scatter; BFP, blue fluorescent protein.

https://dx.doi.org/10.21037/tcr-23-909

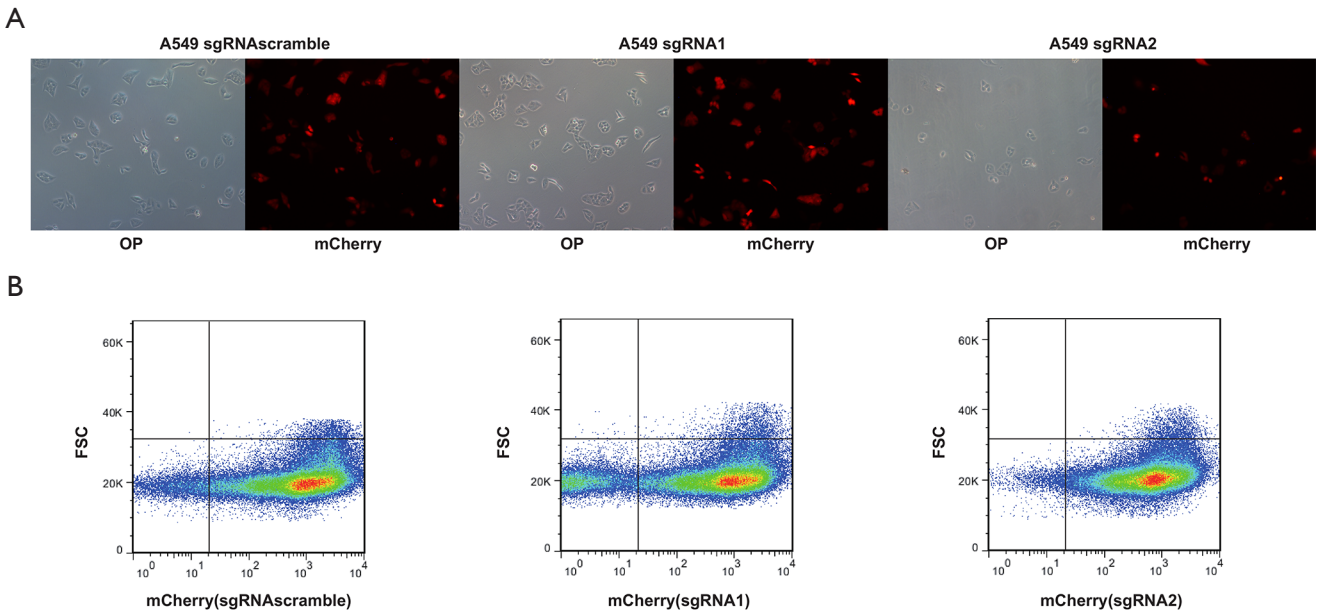

Figure S2 A549 cell line with stable expression of *DNMT3A* and sgRNA was constructed. (A) pgRNAmodified-sgRNAscramble/pgRNA-modified-sgRNA1/pgRNA-modified-sgRNA2 were transfected stably in A549-*DNMT3A* cell line; Pictures were taken under inverted fluorescence microscope. (B) The mCherry positive cells were screened by ultra-high speed flow cytometry sorting system. OP, optical picture; FSC, forward scatter; sgRNA, single guide RNA.

https://dx.doi.org/10.21037/tcr-23-909